THE ASTROPHYSICAL JOURNAL, 429:465–479, 1994 July 10

THE FRACTION OF MATTER IN VOIDS

JAAN EINASTO,[1] ENN SAAR,[1] MARET EINASTO,[1] WOLFRAM FREUDLING,[2] AND MIRT GRAMANN[1,3]
Received 1993 August 30; accepted 1994 January 7

ABSTRACT

Evacuation of matter from voids is investigated using numerical simulations. Cold dark matter–type and simple power-law models with different density parameters and scales are used. The density distribution of model samples is compared with the distribution of observed samples of galaxies.

Our goal is to restore the *actual* distribution of matter from the *observed* distribution of galaxies as accurately as possible. Based on the assumptions that the dominating constituent of the universe is dark matter, and that in systems of galaxies the dark matter is concentrated approximately as strongly as visible galaxies, we calculate from the discrete distribution of particles and galaxies continuous density fields using a smoothing length not exceeding the characteristic radius of systems of galaxies.

We compare the mass-weighted density distributions of model and real samples and find that they are different. Models contain a smooth population of particles in low-density regions which has no counterpart in the observed distribution of galaxies; in other words, galaxies do not follow the matter distribution in the whole range of densities. This disagreement between modeled matter distributions and the observed galaxy distribution does not depend on the details of the considered models but is a generic feature of the range of models considered in this paper. However, the disagreement is a feature of the smoothing scale we chose to investigate here.

To simulate the observed distribution of galaxies, the distribution of matter in models is truncated at a certain threshold density. We demonstrate that the threshold density is equal to the mean density of matter. Particles in high-density regions can be identified with the clustered population, including dark coronae around galaxies and clusters. Particles in low-density regions form the void population. During the evolution particles flow from low-density regions to high-density ones. In the present epoch approximately 15% of matter lies in voids and 85% of matter forms the clustered population.

This result poses a problem for some cosmological models, since the density of the clustered population is according to available estimates $\Omega_c \approx 0.15$ of the critical cosmological density, and the total density including the matter in voids is $\Omega_{\rm matter} \approx 0.20$. Possibilities to hide some dark matter in intermediate-density regions are discussed.

It is demonstrated that the fraction of matter in the clustered population, F_c, is related to the conventional biasing parameter via $b = 1/F_c$. Thus, the biasing parameter cannot be considered as a free parameter; its value is determined by the data discussed above. The value of the biasing parameter depends on the smoothing scale; for our adopted scale 1.2 h^{-1} Mpc, $b \approx 1.18$.

Subject headings: cosmology: theory — galaxies: clustering — large-scale structure of universe — methods: numerical

1. INTRODUCTION

Properties of the large-scale structure of the universe are largely determined by the density field. From observations we can find the distribution of matter associated with galaxies, but the mass distribution of the universe can be inferred only indirectly. To find the matter distribution, we must know how much matter belongs to the voids and how matter is distributed.

In early cosmological studies the question whether galaxies follow the matter distribution or not was not discussed. That this is a problem was first recognized from three-dimensional studies of the distribution of galaxies in space (Gregory & Thompson 1978; Jõeveer & Einasto 1978; Tarenghi et al. 1978; Tifft & Gregory 1978; Tully & Fisher 1978). In these papers it was demonstrated that the universe has a filamentary and cellular structure: most galaxies are concentrated into filamentary superclusters, and the space between superclusters is devoid of visible galaxies. On the other hand, numerical simulations available in the late 1970s (Zel'dovich 1978, and references therein) indicate the formation of a network of filaments but reveal also a striking difference between theory and observations. In simulations, a more or less homogeneous population of nonclustered test particles exists in low-density regions, which has no counterpart in the observed distribution.

This discrepancy was discussed by Jõeveer, Einasto, & Tago (1978). They found a filling factor of 0.01 for the matter associated with galaxies and emphasized that since "*it is very unlikely that the process of galaxy and supercluster formation was effective enough to evacuate completely such large volumes as cell interiors*," there must be dark matter in voids.

Quantitatively the difference between the distribution of matter and the distribution of galaxies was demonstrated by the multiplicity test by Zel'dovich, Einasto, & Shandarin (1982, hereafter ZES) and Einasto et al. (1984, hereafter EKSS). This test clearly emphasizes that galaxy formation is biased relative

[1] Tartu Astrophysical Observatory, EE-2444 Tõravere, Estonia; einasto@aai.ee; saar@aai.ee; maret@aai.ee.
[2] Space Telescope–European Coordinating Facility, D-85748 Garching, Germany; wfreudli@eso.org.
[3] Princeton University Observatory, Princeton, NJ 08544; mirt@astro.princeton.edu.

to the mass distribution. ZES also gave an estimate of the fraction of the matter which still resides in low-density regions—about 50%. To estimate the fraction of matter in voids, subsequently other tests were used—the filling factor test and the fraction of isolated galaxies (Einasto & Saar 1987), the percolation test (Gramann 1990), and the void probability function test (Einasto et al. 1991). The results of these tests gave values for the fraction of matter in voids between 0.2 and 0.5, with relatively large scatter.

The evolution of voids has been recently studied by van de Weygaert (1991) and Dubinski et al. (1993). They demonstrated that the density of matter in voids decreases steadily due to the outflow of matter from voids. These numerical calculations are confirmed by observations; Freudling, Martel, & Haynes (1991) have found that galaxies move away from the large void located between the Local and Hercules superclusters. However, the poor resolution of such observed velocity maps does not allow us to investigate a possible difference between the underlying matter distribution which drives the peculiar velocity and the galaxy distribution.

In this paper we investigate this issue using a completely different approach. For this purpose, we have simulated the evolution of the *matter* in voids numerically, using a conventional N-body code. Simulation of the *galaxy* distribution using a combination of gravitational and hydrodynamical codes, such as those by Cen & Ostriker (1992a, hereafter CO; 1992b), Katz, Hernquist, & Weinberg (1992), or Evrard, Summers, & Davis (1994), suggest that while the distribution of galaxies in high-density environments closely follows the matter distribution, there are fewer galaxies than expected from the available matter in low density. Earlier, this was postulated from theoretical considerations by ZES. This observation motivated us to investigate the division of matter between high- and low-density regions and compare it with the observed galaxy distribution.

The paper is organized as follows: In § 2 we discuss observational and model data used. In § 3 we analyze the evolution of the density distribution using models with cold dark matter–type (CDM–type) and simple power spectra of different scales and density parameters. Using a threshold mechanism, we divide the matter into clustered and nonclustered populations, and follow the decrease of the amount of matter in voids. In § 4 we try to answer the question. Which test particles can we use to investigate the overall distribution of matter? In dense regions galaxies seem to be good tracers of the matter distribution, but it is not clear whether galaxies trace the mass in all density regimes. We derive the threshold density of the matter associated with galaxies by comparing simulations with observations using the density distribution test. In § 5 we analyze the evacuation of voids by analytical calculations. In § 6 we consider the linear biasing model. In § 7 we discuss our results.

Throughout this paper, h denotes the Hubble constant in units of 100 km s^{-1} Mpc^{-1}.

2. DATA USED

2.1. *Observational Samples*

The main issue of this paper is the study of the distribution of matter in voids and high-density regions. From earlier studies it is well known that most galaxies are concentrated to filamentary systems and superclusters, and the space between superclusters is almost devoid of galaxies. It is well known that different systems of galaxies define voids of different size. Thus, voids defined by rich clusters of galaxies contain a number of smaller systems and filaments (ZES). Examples are the void between the Local and Hercules superclusters, or the Northern Local void (ZES; Einasto et al. 1994), and the Bootes void (Kirshner et al. 1981). Detailed studies have shown that such large voids are not completely empty; in particular, the Northern Local void is filled with a network of faint galaxy filaments (Jõeveer & Einasto 1978; Freudling, Haynes, & Giovanelli 1988), and in the Bootes void a number of galaxies have also been found (Balzano & Weedman 1982; Zmoody et al. 1987; Peimbert & Torres-Peimbert 1992).

In the present paper we are interested not necessarily in the structure of these large voids, but more generally in low-density regions defined by both luminous and faint galaxies, including dwarfs. To investigate this we need complete data on galaxies up to a fairly faint absolute magnitude limit. For this purpose only nearby regions of the universe can be used, where data on faint galaxies are fairly complete.

We have used a cubic sample around the Virgo Cluster, V20, chosen from the Huchra (1991) compilation of galaxy redshifts, which contains information on all available redshift sources. Data were reduced as described by EKSS. The velocities were corrected for the solar motion and the Virgocentric flow. The dynamic velocities in clusters and rich groups were compressed to eliminate the "finger of God" effect. The sample is absolute magnitude–limited. The sample size L, the absolute magnitude limit M_0, and the number of galaxies N are given in Table 1. The supergalactic coordinates of the center of the sample were taken as follows: $X_0 = 0$, $Z_0 = 0$; the coordinate Y_0 is given in Table 1. The sample consists of galaxies with absolute magnitudes brighter than -15.0 (absolute magnitudes correspond to the Hubble constant $H = 100$ km s^{-1} Mpc^{-1}). In the volume under study this sample contains all dwarf spiral and irregular galaxies observed by Fisher & Tully (1981) and by other authors in radio surveys which have a limiting redshift ~ 3200 km s^{-1}. Thus the Local Supercluster is the only region where almost complete data are available on relatively faint galaxies for a large region in space.

To study the dependence of statistical properties on the luminosity of galaxies, we have formed also a subsample of galaxies with higher luminosity cutoff; data on this subsample (V20b) are also given in Table 1.

2.2. *Models*

To investigate the evolution of the matter distribution, we have performed a series of three-dimensional simulations using a particle-mesh code with $N = 64^3$ particles in a 64^3 mesh; for details see Gramann (1988). The comoving box sizes were $L = 40$, 60, and 80 h^{-1} Mpc, giving the nominal resolution 0.625, 0.94, and 1.25 h^{-1} Mpc, respectively.

Models have been designated as follows: the first number shows the size of the computational box in tens of megaparsecs, the second number indicates the absolute value of the effective spectral index in the computational box. To avoid too

TABLE 1

SUMMARY OF PARAMETERS OF OBSERVED SAMPLES

Sample	L (h^{-1} Mpc)	N	M_0	Y_0 (h^{-1} Mpc)	σ_8	$\sigma_{1.2}$
V20.....	20	1196	−15.00	15	0.92	4.61
V20b.....	20	627	−17.00	15	0.90	4.75

TABLE 2

SUMMARY OF PARAMETERS OF MODELS

Model	Ω	n_3	L (h^{-1} Mpc)	N	σ_8	$\sigma_{1.2}$
M41e	1.0	≈ -1	40	262,144	0.63	3.50
M41e.1	1.0	≈ -1	40	225,185	0.74	4.08
M41	1.0	≈ -1	40	262,144	0.90	4.73
M41.1	1.0	≈ -1	40	232,478	1.02	5.35
M42e	0.2	≈ -2	40	262,144	0.68	3.32
M42e.1	0.2	≈ -2	40	214,936	0.85	4.09
M42	0.2	≈ -2	40	262,144	0.80	4.17
M42.1	0.2	≈ -2	40	218,991	0.97	5.03
M61e	1.0	-1	60	262,144	0.75	3.72
M61	1.0	-1	60	262,144	0.98	4.74
M62e	1.0	-2	60	262,144	0.83	3.33
M62	1.0	-2	60	262,144	1.57	5.85
M81e	1.0	≈ -1	80	262,144	0.54	3.09
M81e.1	1.0	≈ -1	80	215,468	0.72	3.81
M81	1.0	≈ -1	80	262,144	0.81	4.27
M81.1	1.0	≈ -1	80	227,397	0.94	4.95
M82e	0.2	≈ -2	80	262,144	0.80	3.19
M82e.1	0.2	≈ -2	80	211,498	1.02	4.04
M82	0.2	≈ -2	80	262,144	1.21	4.99
M82.1	0.2	≈ -2	80	221,902	1.45	5.92

complicated numbering of models, other parameters involved (the density parameter and the form of the power spectrum) are not included in model designation; they can be found in Table 2 and are briefly described here. For the density parameter we have used two values, a closed universe $\Omega = 1$ (models M41, M61, M62, and M81); and a low-density universe with matter density $\Omega_m = 0.2$ and the density associated with cosmological constant $\Omega_\Lambda = 0.8$ (models M42 and M82). In models M41, M42, M81, and M82 a CDM-type initial spectrum was given according to the formula used in Gramann (1988). Models M61 and M62 have pure power-law spectra with indices $n = -1$ and $n = -2$, respectively. Initial spectra are plotted in Figure 1. In models M42 and M82 the effective spectral index, $n_{\rm eff}$, throughout the scale interval $L/32 < \lambda < L$ is $n_{\rm eff} \approx -2$; in models M41 and M81 the effective spectral index is $n_{\rm eff} \approx -1$, which justifies the designation of respective models.

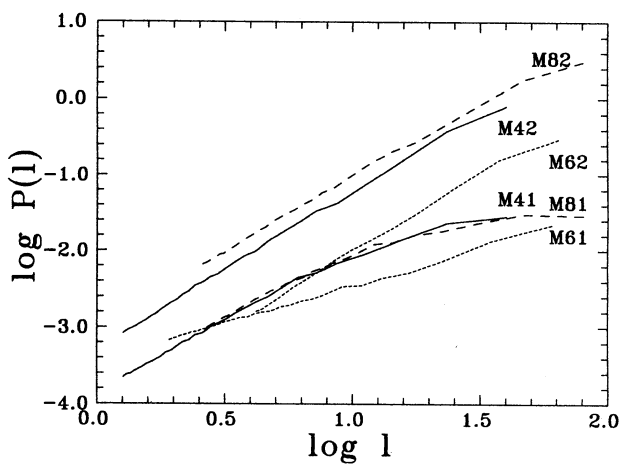

FIG. 1.—Initial spectra of models. As the argument we use the scale $l = 2\pi/k$. Spectra for models M41 and M42 are plotted as solid lines, for models M81 and M82 as dashed lines, and models M61 and M62 as dotted lines.

To get samples similar in size to the observed sample V20, we have divided models M41 and M42 into eight cubic subsamples of size $L = 20\ h^{-1}$ Mpc, and randomly diluted these subsamples to have the same number of objects as the observed sample V20.

To simulate the distribution of the clustered population of matter, models have been truncated at threshold densities $D_t = 1$, 2, and 5 (see below); respective models are designated as M41.1, ..., with similar designations for models M42, M81, and M82.

To follow the evolution of models, we have stored and analyzed data for a number of time steps. Models were evolved until the rms density dispersion reached a value that exceeded the observed value (see below). In the table we give data on two epochs, denoted as M41e and M41 for the earlier and later epochs, respectively, and similarly for the rest of models.

2.3. *The Density Field*

We shall divide the matter into two components, located respectively in high- and low-density regions. The evolution of these two components is different: the matter flows away from low-density regions and concentrates into high-density regions. This difference in the evolution is well known from analytical studies (Zel'dovich & Novikov 1983) and numerical simulations (see van de Weygaert 1991 and Dubinski et al. 1993 for recent papers).

The two regions are also different in their galaxy content. CO have demonstrated that the density of model galaxies drops rapidly with the decrease of the matter density, and below average matter density $D_m = \rho_m/\bar{\rho}_m = 1$ there are practically no galaxies in low-density regions (see Fig. 4*a* in their paper). Our analysis of the density distribution of the galaxy population confirms these theoretical calculations (see the next sections).

The basic constituent of matter in both high- and low-density regions is the dark matter. Visible galaxies can be considered as test particles which indicate also the distribution of the underlying dark matter in the clustered component. It is natural to assign all the matter which is located in systems of galaxies (clusters, groups, galaxies with their dark coronae) to the clustered matter.

We assume that in high-density regions galaxies follow the matter distribution. There are two reasons to do this, one observational and one theoretical. Observationally it is known that the number density of galaxies in groups and clusters of galaxies follows the total spatial density of matter (Vennik 1986; Hughes 1989). Theoretically CO have shown that in high-density regions the density distribution of simulated galaxies follows closely the total matter density.

Now we turn to low-density regions. Theoretical results by CO show that when the spatial density decreases below the mean density, then the density of galaxies drops rapidly to zero. This result is confirmed by observational evidence mentioned in § 1 and discussed in more detail in the following sections. Initially positive and negative density fluctuations are of equal amplitude and scale; thus the mean density level divides the matter naturally into similar high- and low-density regions. We can use this mean density level to divide the matter into clustered and nonclustered components. In principle, during the evolution this threshold density can change; thus we take the present value of the threshold density as a parameter which must be derived from the comparison of models with observations.

Based on the considerations discussed above, we assume that the total density of matter ρ_m is equal to the clustered matter density, ρ_c, or to density of matter in voids, ρ_v:

$$\rho_m = \begin{cases} \rho_c & \text{if} \quad \rho_m \geq \rho_t \,, \\ \rho_v & \text{if} \quad \rho_m < \rho_t \,; \end{cases} \tag{1}$$

here ρ_t is the threshold density which divides the matter into the clustered and nonclustered (void) components. Instead of absolute densities we can also use relative densities in units of the mean matter density, $D = \rho/\bar{\rho}_m$ and $D_t = \rho_t/\bar{\rho}_m$. Calculations by CO show that in models the transition from the clustered to the nonclustered component is not so sharp as indicated in our equation (1) (see also Figs. 5 and 6 for the observed distribution of the matter density); thus this formula must be taken as an approximation.

The observed density field corresponds to the location of galaxies in the redshift space; in models we calculate the density field in the real space. This raises the question whether the density fields determined in the different spaces are comparable. To investigate this problem, we have calculated the density distribution function both for the real space and for redshift space in models. These calculations demonstrate that the density distributions are practically identical (in the critical region $D \approx 1$ the change $\Delta F_c \approx 0.002$). This result is expected, since the velocities of particles are determined by the spatial derivative of the gravitational potential, which is a very smooth function and does not change rapidly around dense systems of galaxies. For this reason, particles in the critical transition region have identical velocities; in other words, the use of the real space instead of the redshift space in models does not move particles from the clustered component into the nonclustered component and vice versa, and the density distribution is not distorted. Thus we can ignore the difference between the real space and the velocity space.

2.4. *The Smoothing Length*

The input data in both models and observations are catalogs of particles or galaxies. Our basic test is the comparison of density fields of models with observations. Thus we have to find the continuous density fields from discrete distributions of model particles or galaxies. The problem here is which smoothing method to use in order to avoid a distortion of the true density distribution.

The dominating constituent in the mass budget of the universe is dark matter which consists of particles of very low mass. With high accuracy the *actual* distribution of dark matter can be considered as a continuous function with density enhancements around galaxies and in systems of galaxies. These density enhancements define the division of the dark matter into high- and low-density components.

For smoothing we have used the CIC scheme with a certain smoothing length. Formally, the smoothing length is a free parameter of the problem. In previous studies of the density field, usually fairly large smoothing lengths were used. In the present study we chose to use a much smaller smoothing length for the following reason.

From observations we know that dark coronae of galaxies have a characteristic radius of several hundred kiloparsecs, and galaxy systems have a radius of the order of $1\ h^{-1}$ Mpc (see below). When we use a smoothing length much larger than the size of galactic coronae or systems of galaxies, then a part of the particles located actually in high-density regions are moved into low-density regions and vice versa. To get the true distribution of densities, we want to avoid this mixing of different components. The smallest structural units we consider in this paper are groups and clusters of galaxies, since the majority of galaxies are situated in groups, clusters, and filaments joining them (see EKSS). Radii of groups, clusters, and filaments of galaxies vary in rather narrow lumits from ≈ 0.5 to $\approx 1.5\ h^{-1}$ Mpc (EKSS). To avoid any broadening of the actual density distribution, the smoothing length should be at least 3 times smaller than the scale of systems of galaxies. In this case we encounter, however, another problem. If the smoothing length is considerably smaller than the mean separation between particles in the sample, then the smoothing yields not a continuous density field but a number of isolated density peaks around particles.

Thus, as a compromise between the theoretically preferred and practically possible values, we use the same smoothing length as the characteristic size of systems of galaxies. The distribution of dark matter in groups and clusters of galaxies follows the distribution of visible galaxies (Vennik 1986; Hughes 1989), and we can take the smoothing length equal to the mean value of radii of clusters and groups, $\approx 1.2\ h^{-1}$ Mpc (EKSS). In this case, the clustered and nonclustered matter will not be mixed by excessive smoothing. An independent motivation for the choice of the smoothing scale is the simulation by CO. These authors found a significant deviation of the galaxy distribution from the matter distribution for a $1\ h^{-1}$ Mpc Gaussian smoothing window, which is smoothed away when a much larger smoothing length scale is used.

To investigate the influence of the exact choice of the smoothing length on the results discussed below, we have performed calculations with different smoothing lengths within the range allowed by sizes of systems of galaxies, namely, 0.6, 1.2, and $1.6\ h^{-1}$ Mpc. Absolute values of various statistics used depend slightly on the smoothing length. In this paoper we are mainly interested in model statistics relative to observations. When model and observed statistics are treated in a similar fashion, results are almost independent of the smoothing length.

To see what happens with a larger smoothing length, we have used a $8\ h^{-1}$ Mpc Gaussian smoothing window in models and in a larger observational sample the Local and Hercules superclusters. In this case, groups and clusters of galaxies disappear completely, and only large over- and under density regions are seen. Most rich clusters (found by small-scale smoothing) are located in high-density regions, but a number of smaller groups and clusters are also situated in low-density regions. Such an approach is useful in studying superclusters of galaxies and large underdense regions between superclusters. However, the density distribution found by large-scale smoothing is very different from the actual density distribution, which by definition is known in the case of the models. Therefore, such a larger smoothing scale smoothes away the signal we are looking for and which is discussed in detail in § 4.

3. EVOLUTION OF VOIDS: NUMERICAL SIMULATIONS

3.1. *Evolution of Voids*

We have followed the density evolution of matter in voids. As discussed above, the mean density level divides the matter naturally into the low- and high-density regions. Since initial positive and negative density fluctuations are similar and interchangeable, the amounts of matter in the two regions are

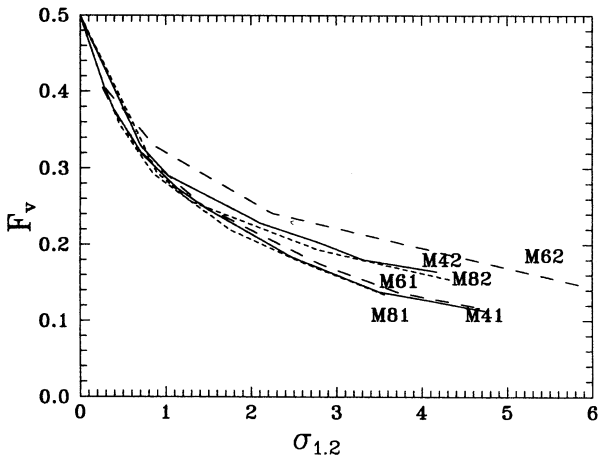

FIG. 2.—Fraction of matter in voids, F_v, is shown as a function of the rms dispersion of relative density fluctuations, $\sigma_{1.2}$. Curves for models M41 and M42 are plotted as solid lines, for models M81 and M82 as short-dashed lines, and for models M61 and M62 as long-dashed lines.

equal. For this reason we have used this fixed threshold density $D_t = 1$ to divide the matter into components. During the evolution the fraction of matter in voids, F_v, decreases. This process is illustrated in Figure 2.

The rms dispersion of relative density fluctuations grows with expansion factor a, and we can use this dispersion as an argument for the density evolution of matter. We have calculated the rms fluctuations $\sigma_{1.2}$ of relative densities (densities expressed in units of the mean density) using the smoothing length 1.25 h^{-1} Mpc. For comparison with other investigators we have calculated also the conventional dispersion σ_8; both dispersions are given in Tables 1 and 2.

The fraction of matter in voids versus the rms dispersion $\sigma_{1.2}$ is plotted in Figure 2. Figure 2 demonstrates that models with different density parameters Ω, effective power indices, and scales have rather similar rates of the evacuation of voids in terms of the density dispersion. A further discussion of the void evacuation is given in § 4.2.

The density evolution in models is shown in Figure 3. Here we plot the fraction of matter in low-density regions for a

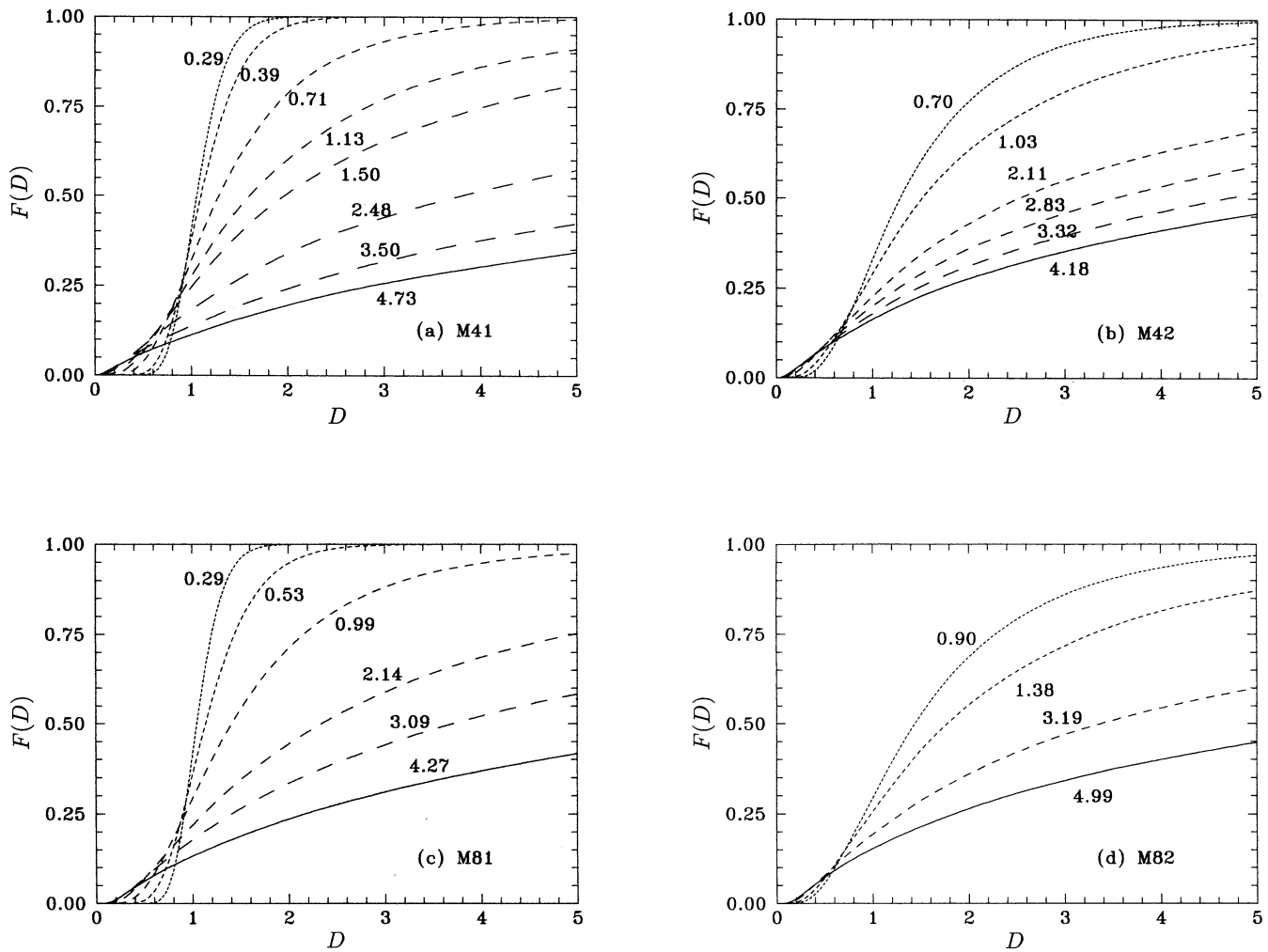

FIG. 3.—Evolution of the integrated density distribution. The fraction of matter in regions with density $D \leq D_t$ is plotted for different epochs, indicated by the rms density dispersion $\sigma_{1.2}$. Panels *a–d* are for models M41, M42, M81, and M82, respectively.

variable threshold density level D, expressed in units of the mean density (the mass-weighted integrated density distribution). Curves correspond to different epochs, shown by the rms density dispersion $\sigma_{1.2}$. Data on models M41, M42, M81, and M82 are given on different panels. We see that particles move gradually into high-density regions, and the fraction of matter in low-density regions drops. The density evolution of models M61 and M62 is very similar and is not plotted here.

We note that the density distribution functions are featureless. Thus the density distribution itself gives no hint at which level we have to make the division between high- and low-density populations. The threshold density which corresponds to actual galaxy populations is to be determined from the comparison of models with observations.

3.2. *Matching Models with Observations*

To identify the present epoch of the model, the rms dispersion of density fluctuations is used. What is needed is the global value of this parameter for a representative sample. Since we use the dispersion averaged over a scale $\sigma_{1.2}$, smaller than used in previous studies, we have to derive it from the observations.

The density dispersions for model samples are given in Table 2. We see that the dispersion depends on the threshold density: samples with higher threshold densities have larger dispersions. The dispersions are almost proportional to the inverse value of the fraction of the clustered matter (see § 6 for further discussion). A high threshold density corresponds to a sample of more clustered galaxies. Bright galaxies are more clustered than normal galaxies, but this phenomenon is observed only for very bright galaxies ($M < -20.0$ for Hubble constant $h = 1$; e.g., Einasto 1991). To find the possible influence of the absolute magnitude on the density dispersion, we have calculated $\sigma_{1.2}$ and σ_8 for subsamples taken at higher magnitude limit, $M_0 = -17.0$. Results show that the dispersion $\sigma_{1.2}$ does not depend on the magnitude limit. This result is in agreement with other studies which show the magnitude dependence only for very bright galaxies.

To find the possible influence of the number of galaxies, we have calculated this dispersion also for full and diluted model samples. Our results show that dilution does not change the density dispersion if it is not excessive. Similarly, Einasto, Klypin, & Saar (1986) found that dilution does not change the correlation function except in extreme cases when the dilution changes the structure (less dense systems disappear completely).

We can adopt $\sigma_8 = 0.9$ in good agreement with the traditional value (Davis & Peebles 1983), and $\sigma_{1.2} = 4.6$. These observed values correspond to the clustered matter in galaxies, and they are to be compared with truncated models $D_t \approx 1$ which correspond best to the distribution of the clustered population.

The rms dispersion for all of the matter can be found by iteration. First we assume that the observed dispersion corresponds to all of the matter, and find from Figure 2 the fraction of matter in voids for this dispersion value. The density dispersion for truncated models scales as (see eq. [31] below) $(\sigma_{1.2})_m \approx (\sigma_{1.2})_c F_c$. From the corrected dispersion we find a new value of F_v and repeat the procedure, which converges rapidly. We find for our adopted value of the fraction of the clustered matter, $F_c = 0.85$ (see below), the rms matter density distributions $(\sigma_8)_m = 0.8$ and $(\sigma_{1.2})_m = 4.0$. In § 4.2 we discuss an independent method to derive the value of the density dispersion for the present epoch. The rms errors of dispersions will be discussed in § 7.3.

4. DISTRIBUTION OF CLUSTERED AND NONCLUSTERED MATTER

4.1. *Influence of the Threshold Density Level*

The density distribution of the clustered matter depends on the threshold density used to divide the matter into clustered and nonclustered components. This dependence is illustrated in Figure 4. The distribution of test particles in regions above a given threshold density $D > D_t$ is shown. If the threshold density is zero, then we consider all test particles as representatives of the clustered population, and the fraction of particles in systems $F_c = 1$. The respective distribution of particles in simulation is shown in Figure 4*a* ($D_t = 0$). With increasing threshold density we first remove particles from the lowest density regions [Fig. 4*b* ($D_t = 1$)]. At a certain threshold density we exclude the filaments that join clusters, and are left with only well-isolated systems [Fig. 4*c* ($D_t = 5$)].

This figure shows that we can use the threshold density to simulate the distribution of particles associated with galaxies of various luminosity as well as galaxies in systems of different richness. Figure 4*c* ($D_t = 5$) corresponds to clusters of galaxies which are well isolated from each other. A somewhat lower threshold density (and a higher fraction of matter in galaxies) corresponds to bright galaxies which are located not only in clusters but also in cores of groups of galaxies. Such groups populate filaments which join clusters into an infinite network. Dwarf galaxies populate the lowest density regions; they correspond to the smallest value of the threshold density.

The question of which threshold density level corresponds to all galaxies (including faint dwarfs) can be answered by comparing the distribution of model particles with real galaxies using various statistical tests. The zero hypothesis—galaxies follow the matter in the whole density interval—corresponds to the threshold density value $D_t = 0$. Thus the question, Do galaxies follow the distribution of matter? can be reduced to the determination of the threshold density. In the next section we apply the mass-weighted integrated density distribution to compare the observed and model distributions.

4.2. *Density Distribution Test*

We shall now compare the density distribution of models with observations. To make model samples as close as possible to the observed sample, we have used eight diluted subsamples of size $L = 20\ h^{-1}$ Mpc. In Figure 5 we compare model sample density distributions with the observed density distribution, for models M41 and M42. Essentially this figure is an enlargement of the lower left-hand part of Figure 3. As seen from Figure 3, models M81 and M82 have a density distribution which for identical density dispersions is close to the respective distribution for models M41 and M42, and also to the mass distribution for models M61 and M62. Thus the results for models M41 and M42 are representative for all models used in this paper.

The comparison of the density distribution results in Figures 3 and 5 correspond to the zero hypothesis: observations are compared with model samples taken at the zero threshold density level. To see the influence of the density dispersion, we give in Figure 5 the density distribution for two epochs characterized by two values of the density dispersion.

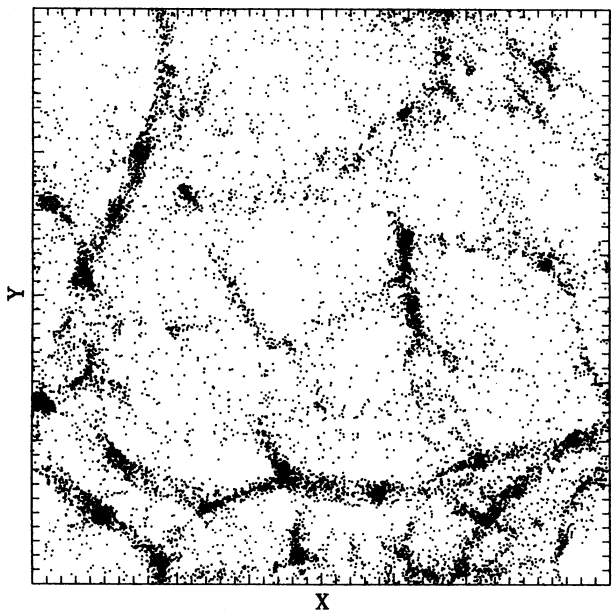

FIG. 4a

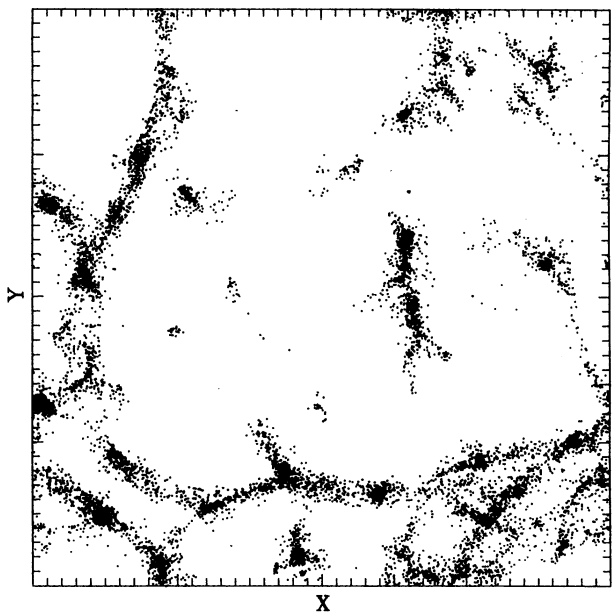

FIG. 4b

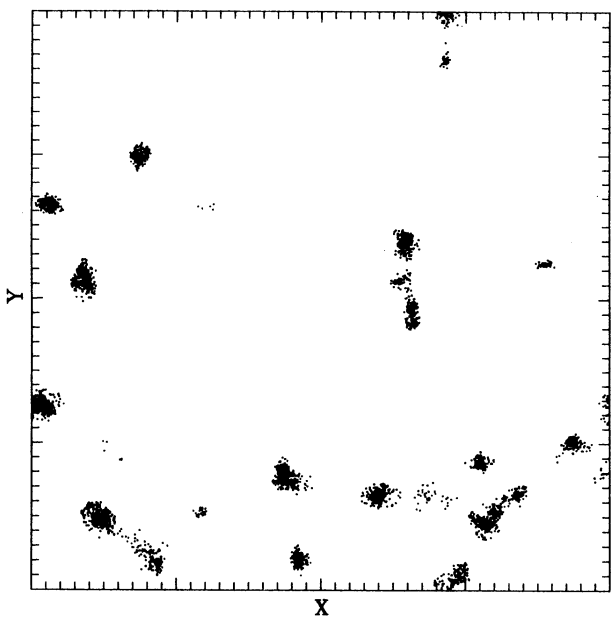

FIG. 4c

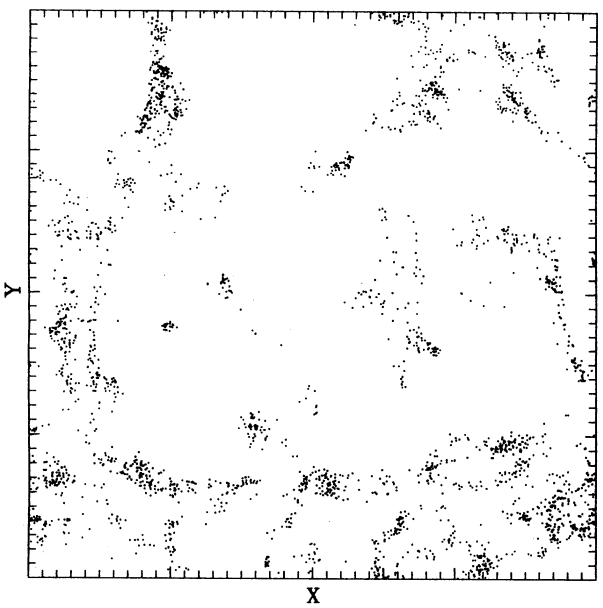

FIG. 4d

FIG. 4.—Distribution of particles in the CDM model M42. A $L/16$ thick slice of side length $L = 40\ h^{-1}$ Mpc has been plotted. Different panels correspond to different threshold densities. Panel a ($D_t = 0$) shows the distribution of all particles in the slice, panel b ($D_t = 1$) the distribution of particles in regions with density $D_m \geq 1$, and panel c ($D_t = 5$) the distribution of particles in high-density regions $D_m \geq 5$. In panel d ($1 < D_t \leq 2$) we show the distribution of particles in the intermediate-density regions, $1 < D_m < 2$.

We see an essential difference between the observed and the model distributions. The model samples have smooth distributions which start from zero and continue smoothly to larger density values. This distribution at low density values is due to the presence of a fairly large fraction (about 15%) of particles in low-density regions, $D < 1$. The observed mass-weighted distribution $F(D)$ becomes significantly larger than zero only at $D \geq 1$. This is the manifestation of the fact that the observed sample does not contain particles in low-density regions. Individual model subsamples have different fractions of particles in high-density regions and thus have widely different integral density distributions, which leads to a scatter of curves. However, in low-density regions all curves differ from the observed integral distribution by a wide margin.

Model samples can be brought into agreement with observations when we exclude particles from low-density regions of model samples using the threshold mechanism with $D_t = 1$. This threshold density is preferred empirically, since the observed distribution starts just at this density level. The integral density distribution of the truncated model samples is

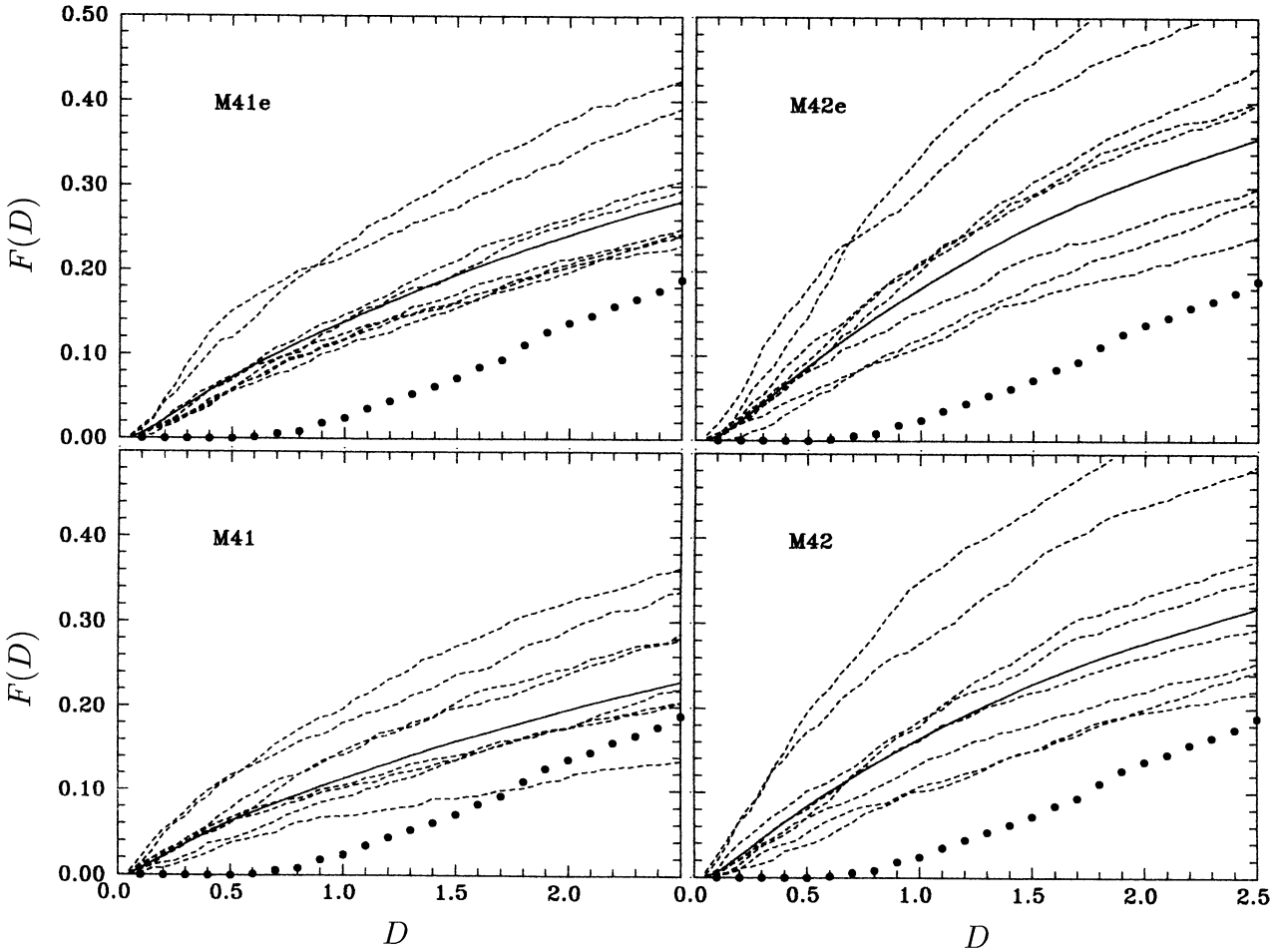

FIG. 5.—Mass-weighted integrated density distribution of models compared with the density distribution of the observed sample V20 (*filled circles*). In different panels data for models M41 and M42 and earlier epoch models M41e and M42e are given. Model samples have been divided into eight subsamples of size $L = 20$ h^{-1} Mpc, and diluted to have in models the same number of particles as in the observed sample; these samples are plotted by dashed lines. Solid lines show the density distribution for full nondiluted models.

shown in Figure 6. Here we also have divided the truncated sample into eight subsamples of size $L = 20$ h^{-1} Mpc and diluted models to have the same number of particles as in the observed sample. Models represent the observed distribution fairly well. There is a scatter of curves for subsamples due to differences in the density distribution in the high-density region. At low densities all model curves are close to the observed one.

Different panels demonstrate the mass-weighted integral density distribution for different models and epochs. The early-epoch models M41e and M42e correspond to the rms density dispersions $\sigma_{1.2} = 3.5$ and 3.3, respectively, whereas the basic models have dispersions $\sigma_{1.2} = 4.7$ and 4.2, respectively (see Table 2). We see that when the density dispersion is less than the observed value (reduced to the matter density distribution), most individual curves of the density distribution lie systematically higher than the observed one. Similarly, when the model density dispersion is higher than the observed value, then model curves lie preferentially below the observed curve.

For comparison, we plot the density distribution in nondiluted full samples in Figure 5 with solid lines and in nondiluted truncated samples in Figure 6. We see that the density distribution of full samples lies just in the middle of the distributions for diluted smaller subsamples. This demonstrates that the division of a sample into subsamples and the dilution do not change the mean density distribution. We can use the mean density distribution of truncated model samples to derive the model which best reproduces the observed density distribution. Using this method, we get the best-fit model epochs (in terms of the rms density dispersion of the full model) 3.26, 4.04, 3.97, and 4.84, respectively, for models M41, M42, M81, and M82. The mean value with its standard deviation is 4.0 ± 0.6. This value coincides with the value directly calculated from observations and reduced to the matter density dispersion.

In spite of differences in the distribution function at larger density values in the critical low-density region, all models have almost identical behavior—they start as the observed curve at the density value $D = 1$. This shows that we can reject the zero hypothesis and adopt the hypothesis that galaxies represent the distribution of matter only in high-density regions.

4.3. *Mean Value of the Threshold Density and the Fraction of Matter in Voids*

We can get an observational estimate of the threshold density by fitting data on sample V20 to a straight line. It crosses the x-axis at $D_t = 0.88 \pm 0.05$. A similar procedure

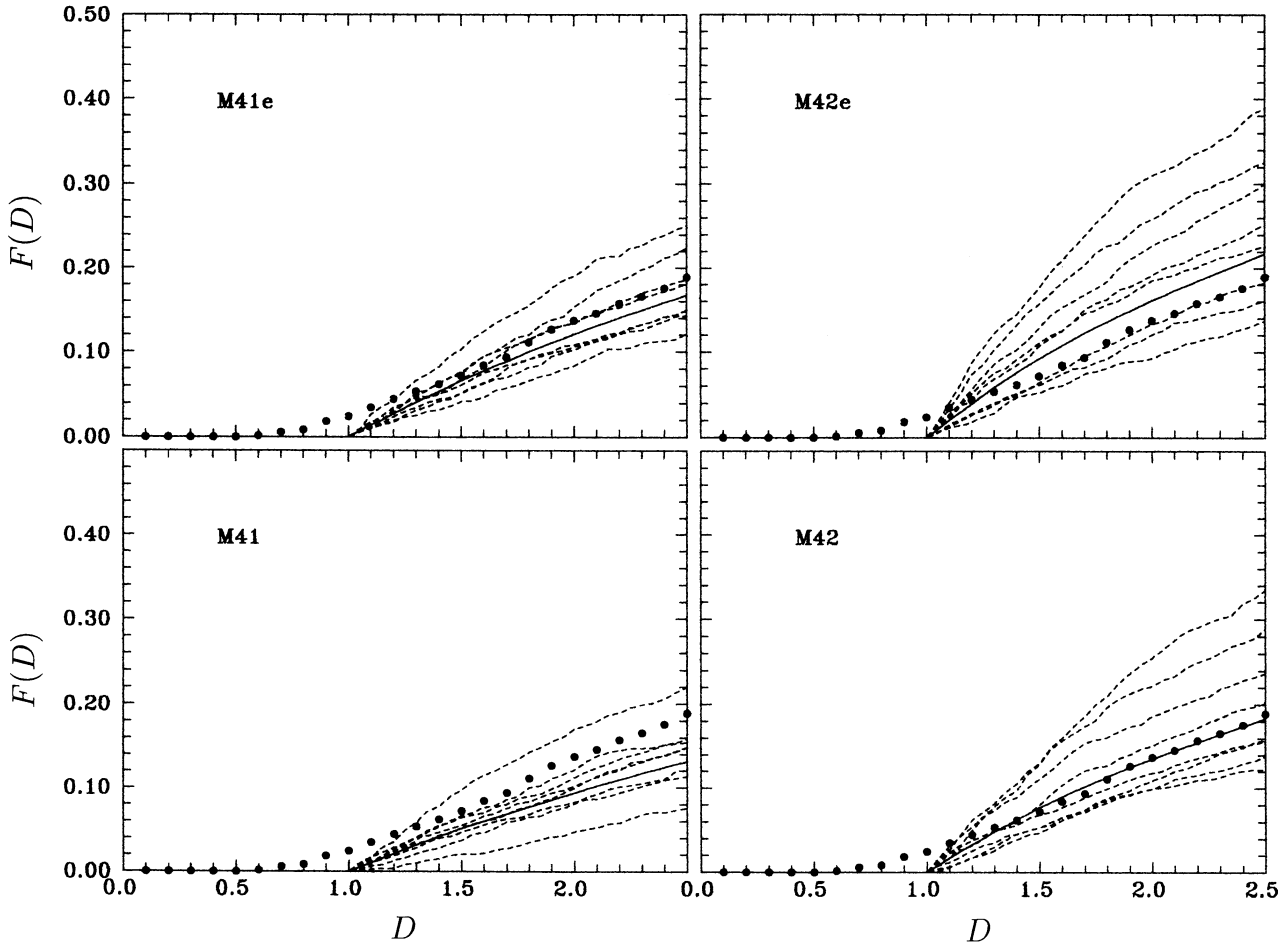

FIG. 6.—Mass-weighted integrated density distribution of truncated models compared with the observed sample V20. Particles from low-density regions $D < 1$ have been removed; the sample has been divided into eight subsamples which have been diluted as in the previous case. Designations are as in Fig. 5.

applied to model data with $D_t = 1$ yields $D_t = 0.97 \pm 0.06$. The difference between the fitting value and the actual one is due to the departure of the data from a straight line. Applying the respective correction to the observed value, we get, for V20, $D_t = 0.91 \pm 0.08$, which within the errors coincides with the theoretically preferred value $D_t = 1$. Thus we can adopt a rounded value for the observed sample, $D_t = 1.0 \pm 0.1$. This method of determining the threshold density of the clustered matter is model-independent.

From Figure 2 we can derive by interpolation the fraction of matter in voids for the adopted density dispersion and threshold density levels. The figure demonstrates that the fraction of matter in voids is systematically lower in models M41 and M81. These models differ from models M42 and M82 in two respects: they have a higher mean density and a flatter spectrum. Models M61 and M62 were generated specifically to clarify this problem; both have closure density, but each has a different spectral index. The density distribution in model M61 is close to the distribution in models M41 and M81, and that in model M62 is close to that of models M42 and M82. Thus these models show that the principal factor, which determines the rate of void evacuation, is the power spectrum index. Models with flatter spectra evolve more rapidly for a given rms dispersion of density fluctuations.

Presently we have no firm reason to prefer one of the above models; moreover, the difference between models is rather small, and thus we adopt the mean value of F_v from all six models, $F_v = 0.15 \pm 0.02$. This error is given by the scatter of individual values. A detailed discussion of errors is given in § 7.3; with all error sources considered, we get a rms error ± 0.05. The corresponding fraction of clustered matter for our chosen smoothing scale is

$$F_c = 0.85 \pm 0.05 .$$

5. EVOLUTION OF VOIDS: ANALYTICAL CALCULATIONS

As seen from the estimates given above, the fraction of matter in voids is far too small to close the universe (either $\Omega = 1$ or $\Omega + \Omega_\Lambda = 1$). Because these numbers have been obtained on the basis of numerical simulations of model universes, it would pay to check them by independent estimates.

For this we need to find the evolution law of density in a void. If we knew the behavior of the density contrast $\delta_v(t)$ (the subscript v denotes "void"), we could take it as a rough estimate for the quantity F_v describing the fraction of mass in voids. Since the density distribution in voids is rather flat in later stages, and voids cover by far the major part of the space, we may hope that this estimate will be good enough.

In order to get the density behavior in a void, we could use two exact nonlinear solutions—that of one-dimensional per-

turbations and a spherical top-hat perturbation—that describe the typical geometry of the elements of structure. Certainly the main problem in void evolution is the expansion of voids that depends on their density profile; this topic has been covered well by Bertschinger (1985) and recently by van de Weygaert (1991) and Dubinski et al. (1993). If we are interested only in the behavior of the central density of a void, we may reduce our problem to a local analysis.

In the one-dimensional case (unidirectional expansion; density and velocity profiles depend on one spatial coordinate only) the Lagrangian displacement amplitude $b(t)$ of a particle,

$$\bar{x}(t) = \bar{q} + b(t)v(\bar{q}) , \tag{2}$$

oberys the (exact) equation (Buchert 1989 and references therein)

$$\ddot{b} + 2H\dot{b} - 4\pi G\bar{\rho}b = 0 . \tag{3}$$

Here $H = \dot{a}/a$ is the Hubble function and $\bar{\rho}$ the mean density of the universe. This equation coincides with the linear equation for density evolution and can be solved exactly for Friedmann-Lemaître cosmologies.

The important point here is the relation between the displacement amplitude and the density contrast that can be written as

$$D(t, \boldsymbol{r}) = 1 + \delta(t, \boldsymbol{r}) = \frac{1}{1 - \delta_i(\boldsymbol{r})b(t)/b_i} , \tag{4}$$

where $D(t, \boldsymbol{r})$ is the normalized density and we have supposed that the initial density perturbations $\delta_i(\boldsymbol{r}) \ll 1$.

If we consider now two typical initial density perturbation profiles, of the same absolute value of the amplitude extremum δ_i at t_i (and of the same scale), but of different signs, then at the moment t_f, when $b(t_f) = b_i/\delta_i$, the positive density perturbation will formally diverge (the first crossing). This moment is usually loosely identified as the epoch of structure formation. At the same moment the normalized minimum density of the negative perturbation, $D_v(t)$, and the corresponding density contrast, $\delta_v(t)$, reach the values

$$D_v(t) = 1 + \delta_v(t) = 0.5 . \tag{5}$$

The subsequent evolution of D_v depends on the model; for the simplest $\Omega_0 = 1$ model we get

$$D_v(x) = \frac{1}{1 + x_f/x} , \tag{6}$$

where $x = 1 + z$ is the redshift parameter and x_f describes the epoch of structure formation. For the present moment $D_v = 1/(1 + x_f)$, and $F_v \approx D_v$, if we consider the density throughout all voids to be close to D_v and suppose that voids cover most of the space.

Now, unidirectional expansion clearly underestimates the evacuation rate of a void. While high-density structures frequently resemble walls, a typical void is rather spherical, and nonspherical voids get more spherical in the course of expansion (see Bertschinger 1985). Because of this we can use an old trick (Zel'dovich & Novikov 1983) of treating the large-scale perturbations as pieces of cosmological models of different density. This also means that we ignore the coordinate dependence of the perturbed density.

Let us consider simple universes with $\Omega_\Lambda = 0$ and $\Omega_0 = 1$. If we describe our void as a cosmological model of lower density with the present density parameter Ω_v, then the age T_v of that model at the redshift parameter x_v is (Zel'dovich & Novikov 1983, chap. 3, § 4)

$$T_v = \frac{2}{3H_0\Omega_v^{1/2}x_v^{3/2}} \tag{7}$$

(this relation is valid for all values of Ω_v if the universe is young enough, $x \gg 1$), and its density changes as

$$\Omega_v(x_v) = 1 - \frac{1 - \Omega_v}{1 + \Omega_v(x_v - 1)} \tag{8}$$

(we mean by Ω_v the value of the density parameter at the present epoch $x_v = 1$).

The last formula gives us the amplitude of the negative density contrast as

$$-\delta_v(x_v) = \frac{\bar{\rho} - \bar{\rho}_v}{\bar{\rho}} = 1 - \Omega_v(x_v) = \frac{1 - \Omega_v}{1 + \Omega_v(x_v - 1)} \tag{9}$$

(the density parameter of the background model is $\Omega = 1$). We shall also need a formula for the age of the background model T:

$$T = \frac{2}{3H_0 x^{3/2}} , \tag{10}$$

where x is the "real" redshift parameter.

While voids usually become more spherical during their evolution, the first structure will probably form by one-dimensional collapse. This allows us to use equation (4) to describe the evolution of the density contrast of generic perturbations of positive amplitude in our main $\Omega = 1$ universe at early times, and to write

$$\delta_c = \frac{1}{1 - x_f/x} - 1 \approx \frac{x_f}{x} . \tag{11}$$

Here, of course, the epoch of structure formation depends on spatial coordinates, $x_f = x_f(\boldsymbol{r})$. We shall select the value of x_f that describes the positive density perturbations of the same initial spatial scale as our voids, and of maximum amplitude, and shall call this X_f—the epoch of formation of large-scale structure. As we have to compare perturbation amplitudes at equal times, we get from the requirement $T_v = T$ the relation between redshifts

$$x_v = x(\Omega_v)^{-1/3} . \tag{12}$$

Comparing now the amplitudes of density perturbations of different sign at early times, as we did before, and using the fact that both $x_v \gg 1$ and $\Omega_v x_v \gg 1$, we obtain an implicit formula for Ω_v:

$$X_f = \frac{1 - \Omega_v}{\Omega_v^{2/3}} . \tag{13}$$

Any assumption about the epoch of formation of the large-scale structure X_f will give us a value of the present normalized density in voids, Ω_v, and this parameter can be used as an estimate for the fraction of matter in voids F_v as before, but in this case for a large-scale structure consisting of spherical voids and of superclusters that had planar geometry at their formation.

Similar estimates can be made for models with a cosmological constant. The solution for the amplitude $b(x)$ is well

known (Peebles 1980, chap. 4, § 13). The growing mode of the solution can be written as (Saar 1973)

$$b(x) = g(x) \int_x^\infty \frac{y\,dy}{g(y)^3}\,, \tag{14}$$

where we have introduced the normalized Hubble function $g(x) = H(x)/H_0$ [the Hubble function itself is defined as $H(t) = \dot{a}(t)/a(t)$].

For a Friedmann-Lemaître model this function is given by

$$g^2 = \Omega x^3 + (1 - \Omega - \Omega_\Lambda)x^2 + \Omega_\Lambda\,, \tag{15}$$

and Ω and Ω_Λ are the values of the normalized density and the cosmological constant at the present time. We shall consider only flat model universes, where $\Omega + \Omega_\Lambda = 1$, and, consequently,

$$g^2 = \Omega x^3 + 1 - \Omega\,. \tag{16}$$

For early times (large x) we get

$$b(x) = \frac{2}{5\Omega x}\,, \tag{17}$$

and the density contrast of generic positive perturbations δ_c is related to the redshift parameter of structure formation x_f by

$$\delta_c(x) = \frac{2}{5\Omega x b(x_f)} \tag{18}$$

[$\delta_c(x, \boldsymbol{r})$ is a function of spatial coordinates, of course, but this is taken care of by $b(x_f, \boldsymbol{r})$]. We can also easily calculate the underdensity of voids, using the density evolution law (Saar 1973)

$$\Omega(x) = \frac{\Omega x^3}{g^2} \tag{19}$$

and the fact that the cosmological constant for both models is the same. We use the formula for the age of the universe (eq. [7]) to get the relation between the redshift parameters of different models, as at early times the cosmological constant does not influence the expansion of the universe. The function g^2 is given by equation (16) for our main universe, and by equation (15) for the void. Finally, we get the expression for the absolute value of the underdensity contrast (at early times):

$$-\delta_v(x) = \frac{\Omega(x) - \Omega_v(x)}{\Omega(x)} = \frac{1 - \Omega_v - \Omega_\Lambda}{\Omega^{1/3}\Omega_v^{2/3}}\,. \tag{20}$$

As usual, we suppose that the over- and underdensity amplitudes (eqs. [18] and [20]) have to be equal (this is the case for Gaussian perturbations, at least), and this gives us the equation we need:

$$\frac{\Omega - \Omega_v}{\Omega^{1/3}\Omega_v^{2/3}} = \frac{2}{5\Omega b(x_f)} \tag{21}$$

(we have also used the fact that $\Omega + \Omega_\Lambda = 1$). It will look better if we use the normalized void density ω:

$$\omega = \Omega_v/\Omega\,. \tag{22}$$

The equation for this density can be written as

$$\omega + f(\Omega, x_f)\omega^{2/3} = 1\,, \tag{23}$$

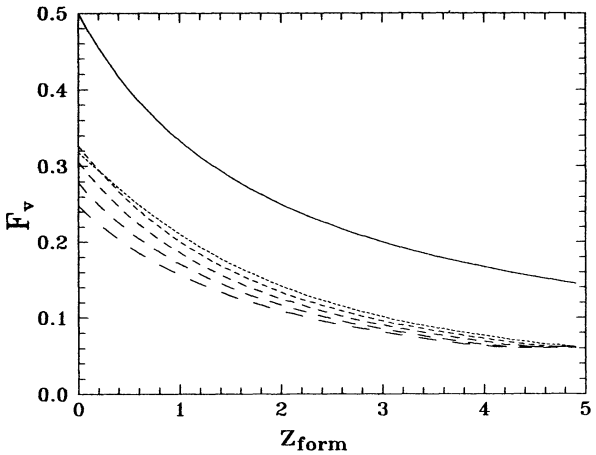

FIG. 7.—Fraction of matter in voids F_v vs. the redshift of the formation of structure, z_{form}, for linear voids and walls (*solid line*) and for spherical voids and dense walls. Lines of increasing dash length indicate models with density parameter $\Omega_0 = 0.2$, 0.4, 0.6, 0.8, 1.0. The density of matter in voids in the model can be calculated from the fraction of matter as follows: $\Omega_v = F_v\Omega_0$.

where the function f comes from equation (18):

$$f(\Omega, x_f) = \frac{2}{5\Omega b(\Omega, x_f)}\,. \tag{24}$$

As before, we shall use Ω_v as an estimate for F_v.

The solution of equation (23) is illustrated in Figure 7, where we have plotted the present fraction of matter in voids F_v for different values of the background density (or cosmological constant, as we suppose $\Omega + \Omega_\Lambda = 1$) versus the redshift of formation of structure. For comparison, we have included the curve for the case of unidirectional expansion of voids (for $\Omega = 1$), too. If we fix the fraction of matter in voids, we can find a range of suitable structure formation times in our simple models (for $F_v = 0.15$, z_f lies in a reasonable interval 1.0–2.0). We have to bear in mind, however, that this has been done at the expense of introducing the cosmological constant, that may be not a popular move. On the other hand, these models can reconcile the inflation scenario requirement of flat space sections ($k = 0$) with the small observed void density.

6. THE LINEAR BIASING MODEL

The fraction of the clustered matter is related to the conventional biasing parameter b. The biasing parameter is usually defined through the galaxy (clustered) and matter density contrast

$$\frac{\rho_c - \bar{\rho}_c}{\bar{\rho}_c} = b\,\frac{\rho_m - \bar{\rho}_m}{\bar{\rho}_m}\,. \tag{25}$$

We can write equation (25) in the following way:

$$\rho_c = \bar{\rho}_c + bF_c(\rho_m - \bar{\rho}_m)\,, \tag{26}$$

using the designation $F_c = \bar{\rho}_c/\bar{\rho}_m$.

In high-density regions the density is much higher than the mean density, and we can neglect mean densities in both sides of equation (26):

$$\rho_c = bF_c\,\rho_m\,. \tag{27}$$

The density of the population cannot be higher than the total density; thus $bF_c \leq 1$. On the other hand, it is unlikely that the

density of matter associated with galaxies decreases with increasing matter density (recall that in the calculation of F_c we attribute all of the matter in high-density regions to the clustered component). Thus we are left with the only possibility,

$$b = \frac{1}{F_c} . \tag{28}$$

The numerical value of b depends of course on the smoothing length used, similar to F_c. In regions of lower density we cannot neglect mean densities, and, since density cannot be negative, we must write the biasing law in density terms as follows:

$$\rho_c = \begin{cases} \rho_m - \bar{\rho}_v & \text{if} \quad \rho_m \geq \bar{\rho}_v , \\ 0 & \text{if} \quad \rho_m < \bar{\rho}_v . \end{cases} \tag{29}$$

We come to the conclusion that the linear biasing scheme, if we apply it to the present epoch when density fluctuations are large, and if we eliminate the physically nonrealistic negative densities, has almost the same form as truncation by a certain threshold density level (see eq. [1]). Here $\bar{\rho}_v$ plays the same role as the truncation density ρ_t in equation (1).

Conventionally biased numerical models are defined through the ratio of galaxian and mass rms density dispersions (i.e., Loveday et al. 1992)

$$b_8 = \frac{(\sigma_8)_c}{(\sigma_8)_m} . \tag{30}$$

Substituting the bias factor with the fraction of matter in galaxies (eq. [28]), and using dispersions averaged over smaller scales, we get the formula

$$(\sigma_{1.2})_c = (\sigma_{1.2})_m \frac{1}{F_c} ; \tag{31}$$

a similar formula is valid also for rms dispersions σ_8. Our calculations show that this formula is satisfied with sufficient accuracy (see Table 2). These formulae are quite general and do not depend on the particular physical biasing mechanism.

7. DISCUSSION

7.1. *Comparison with Previous Determinations*

It is well known that the power spectrum and its Fourier transform, the correlation function, are insensitive to the addition of a smooth homogeneous population of field particles. Such a population corresponds in Fourier space to wavenumber $k = 0$, which means multiplication of the whole spectrum by a constant, so that the shape of the spectrum is not changed.

Most tests previously used to estimate the fraction of the mass in voids suffer from the dependence on the number density of particles, i.e., from dilution. Depending on the dilution level, the signal changes. In the multiplicity function test the signal is strong enough to demonstrate that the zero hypothesis (there is no biasing) is rejected with high probability (see the next section). However, in this method the error in the level of the threshold density to define clustered and nonclustered populations is still large.

Another test previously used to discriminate biased and nonbiased models is the void probability function tests. Einasto et al. (1991) investigated the effect of dilution to the void probability function and found a strong dependence. Thus the error of the determination of the density truncation level is rather large (see Einasto et al. 1991 for details).

A frequently used test is also the filling factor test. The filling factor, $f(D)$, of a sample is defined as the fraction of the total volume where the density is equal to or greater than $D = \rho/\bar{\rho}$ (density is expressed in units of the mean density). Essentially the filling factor is the volume-weighted density distribution. For consistency with the mass-weighted density distribution we can express the volume-weighted density distribution also as the fractional volume where the density is equal to or less than D.

To check the sensitivity of this method, we have made respective calculations for models M41 and M42. It is convenient to calculate the volume in units of grid cells and to take the density in a grid cell equal to its mean value. If the mean number of particles per cell is much greater than unity, then the filling factor is almost independent of the number of particles. In the other case the filling factor depends on the number of particles in samples. We compare model samples with observations; in observed samples the mean number of galaxies per grid cell is smaller than one particle per cell, thus we have to dilute model samples to have a comparable number of objects in observed and model samples.

Density distributions for full samples M41 and M42, and for truncated samples M41.1 and M42.2, are shown in Figure 8 by solid lines; distributions for diluted subsamples of size $L = 20$ h^{-1} Mpc, by dashed lines. We see that the full nondiluted sample deviates strongly from the observed distribution, and the truncated nondiluted sample represents observations well. With dilution the comparison becomes nonconclusive: both the trunctated and the nontruncated models are consistent with the observations over a wide range of threshold densities.

As a further test the fraction of isolated galaxies in diluted models was compared with observations for different neighborhood radii. This test again demonstrates that nontruncated models give a poor fit to observations, but the determination of the correct truncation level is difficult.

The insensitivity to truncation level and strong dependence on the dilution explain the results of Weinberg & Cole (1992), where a number of tests (the correlation function, the void probability function, the nearest-neighbor distribution, and others) were used to compare observed samples with diluted model distributions, and only marginal differences were found. Similarly, Little & Weinberg (1993) used the void probability function to investigate statistical properties of voids in numerical simulations. A wide range of initial Gaussian models were considered, and results were compared with void probability functions of observed samples. Again only marginal differences between biased and unbiased models were found.

This comparison demonstrates that the mass-weighted density distribution is the only test which (1) is sensitive to the truncation level, and (2) is practically independent of the dilution level. In our determination of the truncation level and the fraction of matter in voids we can use only this test.

7.2. *The Zero Hypothesis*

The zero hypothesis corresponds to the case in which all galaxies belong to the clustered component, $F_c = 1$, and thus follow the distribution of matter, or, in other words, the galaxy formation is not biased.

The strongest argument against the zero hypothesis comes from the comparison of the mass-weighted density distribution of real galaxies and unbiased model particles; they are com-

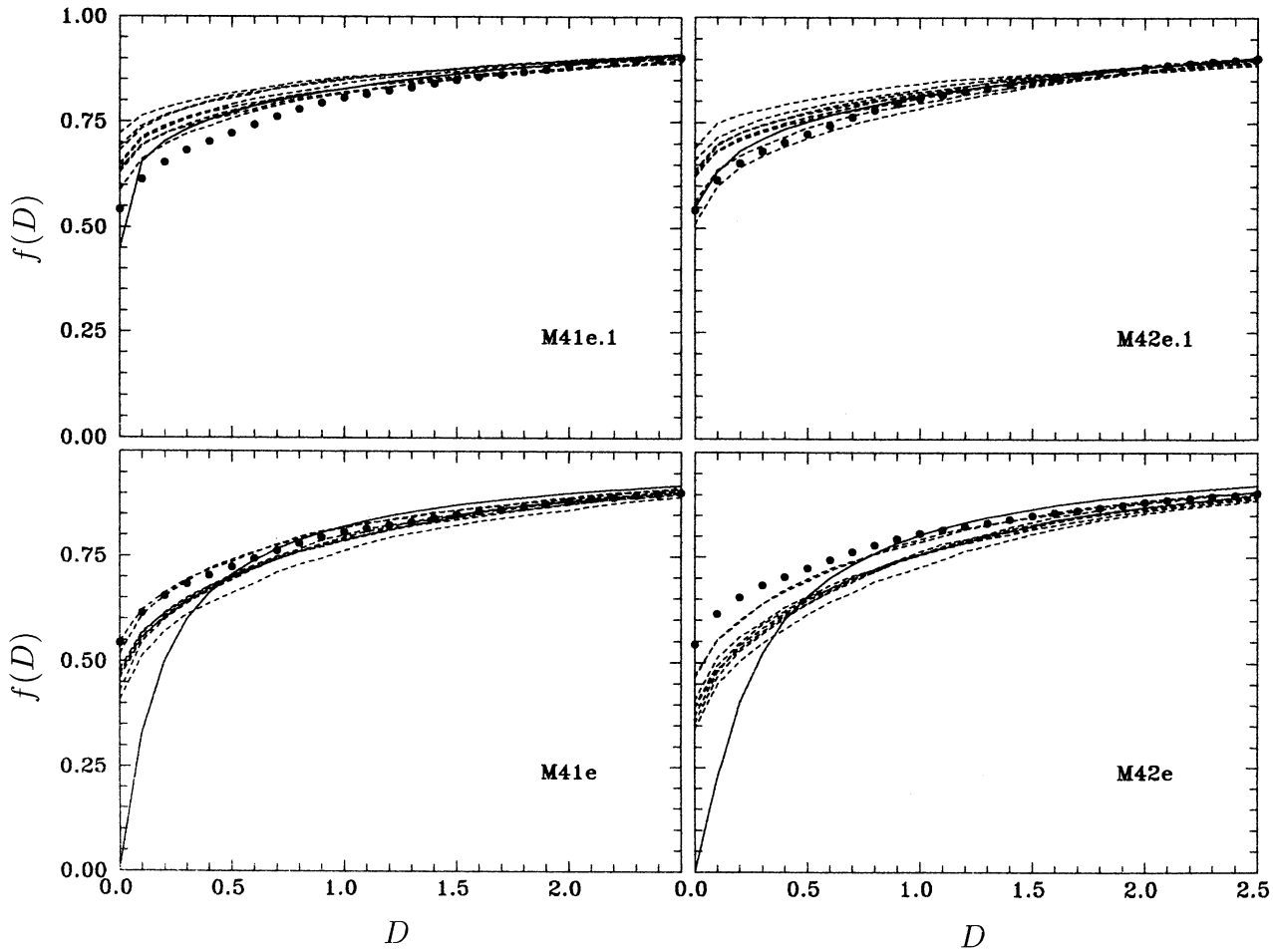

FIG. 8.—Volume-weighted integrated density distribution for eight subsamples of models M41e, M41e.1, M42e, and M42e.1 compared with the observed sample V20. Designations as in Fig. 5.

pletely different. This method is the most sensitive test for comparison of particle distributions in a low-density environment.

Another strong argument for rejecting the zero hypothesis comes from the multiplicity test. As demonstrated by ZES and EKSS, in models there is a numerous population of isolated particles in low-density regions, more or less evenly distributed over the whole low-density region. These particles belong to multiplicity classes 1 (singles) and 2 (doubles). In observations there is a very small population of singles and pairs. At only slightly larger neighborhood radius these galaxies join larger systems, which shows that they form outlying parts of these systems (Einasto 1990). At similar neighborhood radii the population of isolated particles in models is still rather numerous for details see ZES and EKSS).

Thus our present study of the mass-weighted density distribution of real galaxies and model particles, and previous investigation of the multiplicity functions, demonstrate that we can reject the zero hypothesis by a wide margin: galaxies do not follow the matter distribution in the whole density interval.

7.3. *Error Analysis*

We have found an observational estimate for the threshold density to divide the clustered and nonclustered matter, $D_t = 1.0 \pm 0.1$. This value is determined by the mass-weighted density distribution function, shown in Figures 5 and 6. The formal error of this value was determined from the scatter of individual data points on this diagram—how accurately they determine the point of crossing the x-axis. Theoretical modeling of galaxy formation by CO also confirms this threshold density.

The threshold density and rms dispersion of density fluctuations determine the value of the fraction of matter in voids. The error on F_v is due to four factors, the error of the threshold density level to define the clustered matter, the scatter of individual F_v values for different models, the random error in determining the observed value of the density dispersion, and possible systematic deviation of the Virgo sample from a representative sample of the universe.

The error of D_t is so small in comparison with other errors that it plays no role in the error budget of F_v. The second error corresponds to the uncertainty of our knowledge of the initial spectrum of density fluctuations; this error can be found from the scatter of individual values of the filling factor at $\sigma_{1.2} = 4$ and is ± 0.02. The third and fourth errors reflect our uncertainty in determining the rms density dispersion. Unfortunately, the Virgo sample is the only one available with data on faint galaxies needed to derive the density field with higher resolution. To have an idea how much the dispersion can change from place to place, we can use subsamples of model samples and derive for each of them the density dispersion. This exercise gives a rms error for the density dispersion of

± 0.7. Adopting this value for the possible systematic uncertainty of the observed value of $\sigma_{1,2}$, we can calculate also the respective error of F_v using the slope of curves given in Figure 2. The resulting error of F_v is ± 0.02. The random error due to the uncertainty of the rms density dispersion of the observed sample was estimated above using the density distribution test and is ± 0.7, which also leads to an error in F_v of ± 0.02, and to the overall error of ± 0.04. We adopt a round value of the error of ± 0.05.

A comment on the accuracy of our results is related to the determination of the observed power spectrum. From observations one gets the power spectrum using redshifts of galaxies as distance indicators. As emphasized by Kaiser (1987) and Gramann, Cen, & Bahcall (1993), the spectrum in the redshift space is steeper than in the real space. Thus one may assume that the spectral index in the real space is flatter than the observed value, which may lead to a revision of the CDM model to improve its agreement with observations. This adds another uncertainty to our results. Formally we have taken this into account by the rms scatter due to differences in models used.

7.4. *Where Is the Dark Matter?*

The principal result of our study is that the fraction of matter in voids is rather low, $\approx 15\%$ of the total amount of matter or even less. On the other hand, it is well known that the total mass of all systems of galaxies, including their invisible halos, is about 15%–30% of the critical cosmological density (Faber & Gallagher 1979; Davis & Peebles 1983; Gramann 1990; see also Bahcall & Cen 1992). Thus we see here a problem for the standard flat model of the universe. The problem is, of course, not new, but no final answer is available yet.

If one wants to accept the flat model of the universe, one has to hide the dark matter somewhere. Is this possible? Where can the excessive dark matter be located?

If we define low-density regions by the mean density level, then we see no possibility of increasing considerably the fraction of matter in voids. The observed density dispersion indicates that the void evacuation has advanced far enough; thus in voids there is very little room to hide large amounts of unseen matter.

The second possibility for hiding some dark matter is in regions not covered by current mass estimates of the clustered component. Let us assume that the division between the clustered and nonclustered matter is not so sharp as assumed above, and the threshold density for the matter associated with luminous galaxies lies higher, say at $D_t = 2$. In this case not all matter in the intermediate density interval is associated with (mainly dwarf) galaxies, and some matter can escape dynamical estimates of the mass of systems of galaxies. The model distribution of particles between these threshold density levels is given in Figure 4*d* ($1 < D_t < 2$). We see that the intermediate-density matter populates filaments and forms rarefied halos around clusters. This or a similar intermediate-density region seems to be a suitable place to hide some additional dark matter. The prospects for finding large amounts of dark matter in intermediate-density regions are, however, rather limited, since the expected amount of matter between density levels $D = 1$ and $D = 2$ is of the order of 10% of all matter (see Fig. 3 for the distribution of density). This figure shows that about 75% of all matter is located in high-density regions, $D \geq 2$, well within the domain where direct mass estimates of systems of galaxies are possible.

Intermediate-density regions can be populated with extremely faint galaxies. Dwarf galaxies trace the total mass distribution better than bright ones. Because of the importance of this question, several observational programs were started to investigate the distribution of dwarf galaxies. Einasto (1988, 1990), Eder et al. (1989), Schneider et al. (1990), and Thuan et al. (1991) compared the distributions of bright and faint galaxies. A number of tests (multiplicity function and nearest-neighbor tests) were used. Results show that there is no major difference between the distributions of faint and moderately bright galaxies. All galaxies avoid regions between superclusters.

The last possibility for hiding extra dark matter is high-density regions where, according to our calculations, over 75% of all matter is concentrated. How to put dark matter there without luminous galaxies is not clear. One possibility is to assume that in some high-density regions galaxy formation did not take place at all (phantom clusters). But this means that some additional processes must be important which suppress the galaxy formation selectively in some high-density regions. Presently this seems to be an unlikely possibility.

We can summarize by saying that, within the validity of our models, the majority of the matter in the universe lies in regions well above the threshold density $D_t = 2$. This corresponds to compact groups and clusters. If available dynamical data on masses of systems are not completely wrong, we live in a low-density universe.

Some methods yield values up to 1 for the density parameter (Strauss et al. 1992 and Nusser & Dekel 1993, to name only a few recent determinations). Why the discrepancy between different estimates is so large is still unclear.

8. CONCLUSIONS

We use N-body simulations to investigate the evacuation of voids and to derive the fraction of matter situated in voids. Models have been compared with the observed distribution of galaxies in and near the Virgo supercluster, and with analytical calculations. To compare models with observations, we try to reconstruct the actual distribution of mass as accurately as possible using a rather small smoothing length to calculate the continuous density field. Our principal results can be summarized as follows:

1. The comparison of models and observations using their density distributions shows that galaxies do not trace the mass in the whole universe. There exist low-density regions in simulations, whereas real underdense regions are completely devoid of galaxies.
2. Numerical simulations show that the fraction of matter in voids in the present epoch is $F_v = 0.15 \pm 0.05$ for a density field smoothed on a scale of $1.2\ h^{-1}$ Mpc.
3. There is very little room to hide large amounts of dark matter needed to save the flat cosmological model. If a nondetected dark population exists, it should be located in regions where the density exceeds the mean density of matter in the universe.
4. The conventional bias parameter b is simply related to the fraction of matter associated with galaxies, $b = 1/F_c$.

We thank the European Southern Observatory, where a large fraction of this study was performed, for hospitality and a stimulating atmosphere. We note fruitful discussions with David Weinberg and constructive criticism by the anonymous referee.

REFERENCES

Bahcall, N., & Cen, R. 1992, ApJ, 298, L81
Balzano, V. A., & Weedman, D. W. 1982, ApJ, 255, L1
Bertschinger, E. 1985, ApJ, 58, 1
Buchert, T. 1989, A&A, 223, 9
Cen, R., & Ostriker, J. P. 1992a, ApJ, 399, L113 (CO)
———. 1992b, ApJ, 399, 331
Davis, M., & Peebles, P. J. E. 1983, ApJ, 267, 465
Dubinski, J., da Costa, N., Goldwirth, D. S., Lecar, M., & Piran, T. 1993, ApJ, 410, 458
Eder, J. A., Schombert, J. M., Dekel, A., & Oemler, A. 1989, ApJ, 340, 29
Einasto, M. 1988, MNRAS, 234, 37
———. 1990, MNRAS, 242, 56
———. 1991, MNRAS, 252, 261
Einasto, J., Einasto, M., Gramann, M., & Saar, E. 1991, MNRAS, 248, 593
Einasto, M., Einasto, J., Tago, E., & Dalton, G. B. 1994, MNRAS, in press
Einasto, J., Klypin, A. A., & Saar, E. 1986, MNRAS, 219, 457
Einasto, J., Klypin, A. A., Saar, E., & Shandarin, S. F. 1984, MNRAS, 206, 529 (EKSS)
Einasto, J., & Saar, E. 1987, in Observational Cosmology, ed. A. Hewitt, G. Burbidge, & L. Z. Fang (Dordrecht: Reidel), 349
Evrard, A. E., Summers, F. J., & Davis, M. 1994, ApJ, 422, 11
Faber, S. M., & Gallagher, J. S. 1979, ARA&A, 17, 135
Fisher, J. R., & Tully, R. B. 1981, ApJS, 47, 139
Freudling, W., Haynes, M. P., & Giovanelli, R. 1988, AJ 96, 1791
Freudling, W., Martel, H., & Haynes, M. P. 1991, ApJ, 377, 344
Gramann, M. 1988, MNRAS, 234, 569
———. 1990, MNRAS, 244, 214
Gramann, M., Cen, R., & Bahcall, N. 1993, ApJ, 419, 440
Gregory, S. A., & Thompson, L. A. 1978, ApJ, 222, 784
Huchra, J. 1991, redshift compilation (ZCAT), unpublished
Hughes, J. P. 1989, ApJ, 337, 21
Jõeveer, M., & Einasto, J. 1978, in The Large Scale Structure of the Universe, ed. M. S. Longair & J. Einasto (Dordrecht: Reidel), 409
Jõeveer, M., Einasto, J., & Tago, E. 1978, MNRAS, 185, 357
Kaiser, N. 1984, ApJ, 284, L9
———. 1987, MNRAS, 227, 1
Katz, N., Hernquist, L., & Weinberg, D. 1992, ApJ, 399, L109
Kirshner, R. P., Oemler, A., Schechter, P. L., & Shectman, S. A. 1981, ApJ, 248, L57
Little, B., & Weinberg, D. H. 1993, MNRAS, submitted
Loveday, J., Efstathiou, G., Peterson, B. A., & Maddox, S. J. 1992, ApJ, 400, L43
Nusser, A., & Dekel, A. 1993, ApJ, 405, 437
Peebles, P. J. E. 1980, The Large-Scale Structure of the Universe (Princeton: Princeton Univ. Press)
Peimbert, M., & Torres-Peimbert, S. 1992, A&A, 253, 349
Saar, E. 1973, Publ. Astron. Obs. Tartu, 41, 30
Schneider, S. E., Thuan, T. X., Magri, C., & Wadiak, E. J. 1990, ApJS, 72, 245
Strauss, M. A., Yahil, A., Davis, M., Huchra, J. P., & Fisher, K. B. 1992, ApJ, 398, 395
Tarenghi, M., Tifft, W. G., Chincarini, G., Rood, H. J., & Thompson, L. A. 1978, in The Large Scale Structure of the Universe, ed. M. S. Longair & J. Einasto (Dordrecht: Reidel), 263
Thuan, T. X., Alimi, J.-M., Gott, J. R., & Schneider, S. E. 1991, ApJ, 370, 25
Tifft, W. G., & Gregory, S. A. 1978, in The Large Scale Structure of the Universe, ed. M. S. Longair & J. Einasto (Dordrecht: Reidel), 267
Tully, R. B., & Fisher, J. R. 1978, in The Large Scale Structure of the Universe, ed. M. S. Longair & J. Einasto (Dordrecht: Reidel), 214
van de Weygaert, R. 1991, Ph.D. thesis, Leiden Univ.
Vennik, J. 1986, Astron. Nach., 307, 157
Weinberg, D., & Cole, S. 1992, MNRAS, 259, 652
Zel'dovich, Ya. B. 1978, in The Large Scale Structure of the Universe, ed. M. S. Longair & J. Einasto (Dordrecht: Reidel), 409
Zel'dovich, Ya. B., Einasto, J., & Shandarin, S. F. 1982, Nature, 300, 407 (ZES)
Zel'dovich, Ya. B., & Novikov, I. D. 1983, in The Structure and Evolution of the Universe, ed. G. Steigman (Chicago: Univ. Chicago Press)
Zmoody, J. W., Gregory, S. A., Kirshner, R. P., & MacAlpine, G. M. 1987, ApJ, 314, L33